Available online at www.sciencedirect.com

ScienceDirect

www.elsevier.com/locate/jmbbm

Research Paper

The biaxial active mechanical properties of the porcine primary renal artery

Boran Zhou[a], Alexander Rachev[b], Tarek Shazly[a,c,*]

[a]College of Engineering and Computing, Biomedical Engineering Program, University of South Carolina, Columbia, SC 29208, USA
[b]Institute of Mechanics, Bulgarian Academy of Sciences, 1113 Sofia, Bulgaria
[c]College of Engineering and Computing, Mechanical Engineering Department, University of South Carolina, Columbia, SC 29208, USA

ARTICLE INFO

Article history:
Received 15 January 2015
Received in revised form
26 March 2015
Accepted 1 April 2015
Available online 11 April 2015

Keywords:
Vascular mechanics
Active stress
Porcine renal artery
Biaxial active response
Constitutive model

ABSTRACT

The mechanical response of arteries under physiological loads can be delineated into passive and active components. The passive response is governed by the load-bearing constituents within the arterial wall, elastin, collagen, and water, while the active response is a result of vascular smooth muscle cell (SMC) contraction. In muscular blood vessels, such as the primary renal artery, high SMC wall content suggests an elevated importance of the active response in determining overall vessel behavior. This study is a continuation of our previous investigation, in which a four-fiber constitutive model of the passive response of the primary porcine renal artery was identified. Here we focus on the active response of this vessel, specifically in the case of maximal SMC contraction, and develop a constitutive model of the active stress–stretch relations. The results of this study demonstrate the existence of biaxial active stress in the vessel wall, and suggest the active mechanical response is a critical component of renal arterial performance.

Introduction

Arteries under physiological loads exhibit a complex mechanical response that is governed by the geometrical dimensions of the vessel and mechanical properties of arterial tissue. The major load-bearing constituents of the arterial wall, elastin, collagen and water, determine the so called passive mechanical properties of vascular tissue. These constituents ensure integrity of the arterial wall and performance of arterial physiological function as a blood conduit and elastic buffer that reduces the cardiac preload. The smooth muscle cells (SMCs) in the arterial wall have an insignificant effect on the passive properties, but when appropriately activated by mechanical, electrical, or chemical stimuli, they can contract or relax and in turn constrict or dilate the vessel. This phenomenon is termed the active mechanical response. Under normal physiological conditions the SMCs are partially contracted and the vessel manifests basal muscular tone. In concert with the residual strains, muscular tone synergistically contributes to homogenization of the strain and stress distribution across the arterial wall and thus promotes a preferable local mechanical environment for vascular cells (Rachev and Hayashi 1999; Matsumoto et al., 1996). Moreover, the active response occurs as an acute primary mechanism directed to cope with short term

*Correspondence to: 300 Main St., RM A219, Columbia, SC 29208, USA.
E-mail address: shazly@mailbox.sc.edu (T. Shazly).

http://dx.doi.org/10.1016/j.jmbbm.2015.04.004
1751-6161/

changes in flow rate and/or arterial pressure (Brownlee and Langille, 1991; Bayliss, 1902).

The passive and active mechanical response of arteries can be described in several manners. At the overall arterial level, the response is illustrated by pressure–diameter and axial force-axial stretch relationships via data points in the corresponding 2-D planes (Cox, 1975, 1978; Dobrin, 1978). Often as complementary descriptors, several linearized measures in the vicinity of a particular deformed state are calculated based entirely on experimental data, such as compliance and pressure–diameter modulus (called also Peterson's modulus) (Peterson et al., 1960). After appropriate data processing, the mechanical response can be described via stress–strain (or stretch) relationships, which characterize the properties of the arterial tissue. Stresses and strains are calculated after adoption of certain assumptions for the deformation process.

One of the basic tasks of vascular biomechanics is the quantification of the mechanical properties of arteries in terms of continuum mechanics-based constitutive equations. Completion of this task enables the formulation and solution of boundary value problems that provide predictive results for the mechanical response of arteries and for calculation of the stress and strain distribution across the arterial wall. The stress and strain fields determine the local mechanical environment of the vascular cells, the mechanobiological response of which governs arterial homeostasis. Constitutive equations also provide a theoretical framework for design of experimental investigations and processing data from mechanical tests. While the passive mechanical properties of arteries have been thoroughly investigated (Vito and Dixon, 2003; Holzapfel and Ogden, 2010), there are less published studies on mathematical modeling of the active response.

To our knowledge the first continuum-based constitutive model that accounts for the effects of SMCs was proposed in (Rachev and Hayashi, 1999). The model is based on the assumption that when appropriately stimulated, the SMCs produce an active circumferential stress that is additive to the passive stress borne by the extracellular structural constituents. A justification for the stress orientation is the experimental observation that SMCs are aligned mainly in the circumferential direction (Cox, 1978). The magnitude of the active stress is considered dependent on the intensity of stimulation and on the deformed configuration of the artery (Dobrin, 1973, 1983). The model was adopted in subsequent studies that examine the active response of different arterial types, such as basilar artery (Cardamone et al., 2009; Karšaj and Humphrey, 2012; Valentin et al., 2009; Valentin and Humphrey, 2009), and iliac artery (Humphrey and Wilson, 2003). Based on the observation that some SMCs might be oriented not solely in the circumferential direction (Kockx et al., 1993; Dartsch and Hämmerle, 1986), several studies generalized the model by adding an active axial stress (Wagner and Humphrey, 2011; Chen et al., 2013; Agianniotis et al., 2012). The state of knowledge on the active arterial response was summarized recently in a comprehensive review on vascular tissue mechanical models (Kim and Wagenseil, 2014).

Surprisingly there is a lack of constitutive modeling of the active arterial properties of renal arteries. They belong to the class of muscular arteries in which a large portion of the media is occupied by vascular SMCs and the active response is a typical manifestation of arterial performance. An impaired mechanical response, including the active component, is associated with vascular diseases, such as stenosis, hypertension, aneurysm and occlusion, and has increasingly gained recognition as a potential risk factor for kidney failure or cardiovascular morbidity and mortality.

Constitutive equations are quantified from data acquired in appropriate mechanical tests. Briefly, the commonly accepted ex-vivo testing methodology includes the inflation of a tubular specimen performed quasi-statically at fixed levels of axial stretch. First the inflation-extension experiment is run while the SMCs are kept alive and are stimulated to contract. Afterwards, the contractile capability of the muscle is abolished and the mechanical test is repeated. The generated data are processed in the reverse order. First, considering the arterial tissue as an elastic incompressible solid, the passive mechanical properties are determined in terms of a strain energy density function. Next, an analytical form and associated material constants are identified to model the active arterial response. A different approach was recently proposed for constitutive formulation of the axial active stress in mouse aorta (Agianniotis et al., 2012). It allows quantification of the active stress independently of the constitutive modeling of the passive mechanical properties.

This study is a continuation of our previous investigation on the passive mechanical properties of the porcine primary renal artery, which was analyzed in the framework of a four-fiber constitutive model (Zhou et al., 2014). We focus on the description of the active response in the case of maximally contracted SMCs and on the phenomenological constitutive formulation of the active properties by adopting, with some modification, the approach proposed in (Agianniotis et al., 2012).

Methods

Mechanical testing

All tissue handling protocols were approved by the Institutional Animal Care and Use Committee at the University of South Carolina. The right primary renal arteries were dissected from freshly harvested adult (7–12 month old) porcine kidneys obtained at a local slaughterhouse (Caughman's Meat Plant Inc., Lexington, SC). Prior to arterial excision from the intact aorta and kidney, two dots of tissue marking dye were applied close to the proximal and distal ends of the vessel and the distance $l_{in\ situ}$ between the dots was measured using a digital caliper. The artery was then fully isolated from the surrounding organs and cleared of connective tissue, and the distance L^{bt} between the dots was recorded. The in-situ axial stretch ratio with preserved basal muscular tone was calculated as $\lambda^{bt}_{in\ situ} = l_{in\ situ}/L^{bt}$. The arterial sample was then gently rinsed and stored in phosphate buffer saline for transportation to the laboratory. Immediately upon arrival, the sample was cannulated and mounted within a chambered mechanical testing system (Bose BioDynamic 5270, Eden Prairie, MN) configured for inflation-extension testing.

To initiate mechanical testing, the sample was submerged in and perfused with continuously aerated hyperoxic (95% O_2+5%CO_2) Krebs–Henseleit solution at 37 °C and pH of 7.4

(Agianniotis et al., 2012; Huo et al., 2012). A state of maximal SMC contraction was induced by bringing the circulating medium to a 10^{-5} M epinephrine concentration and allowing a 15 min acclimation period to elapse. Both the concentration of epinephrine and the duration of the acclimation period were deemed sufficient for maximal SMC contraction in pilot studies, in which additional stimulant (up to 10^{-4} M epinephrine) or acclimation time (up to 45 min) induced no further modulation of the pressure–outer diameter response of the vessel. The stimulated arterial sample was then mechanically preconditioned at a fixed axial extension corresponding to $l_{in\ situ}$ with 5 inflation-deflation cycles (pressure range of 20–200 mmHg, pressure change rate of 1.5 mmHg/s). Immediately following preconditioning, the sample was retained at $l_{in\ situ}$ and subjected to three consecutive quasi-static inflation-deflation cycles (20–200 mmHg, 20 mmHg steps). The same test procedure was then repeated at fixed axial extensions corresponding to 0.9 $l_{in\ situ}$ and 1.1 $l_{in\ situ}$. At each experimental state defined by the imposed pressure (P) and axial extension (l), the vessel deformed outer diameter (d_o) and axial force (f) were recorded via integrated system components and software (Wintest 4.1, Bose ElectroForce, Eden Prairie, MN and Labview 2010, National Instruments Corporation, Austin, TX).

The passive mechanical response of the sample was next assessed under a fully relaxed SMC state, which was induced by flushing the circulating medium, replacing it with a 10^{-5} M sodium nitroprusside solution, and allowing 15 min for acclimation. Here again, pilot studies were performed to determine the concentration of sodium nitroprusside (up to 10^{-4} M) and acclimation period (up to 45 min) required for induction of complete SMC relaxation. Complete SMC relaxation was verified in additional pilot studies via comparison of the passive vessel response before and after treatment with cytochalasin D (Fonck et al., 2007). Coincident pressure–diameter curves were also observed in these studies, indicating that sodium nitroprusside completely abolished SMC contractility and mitigated the potential for a myogenic response to confound passive experimental measurements. Mechanical preconditioning and passive inflation-extension testing were performed following the methodology described above. A total of five right primary renal arteries ($N=5$) were acquired from five animals and mechanically tested following the described methodology.

Upon completion of active followed by passive mechanical testing, the sample was removed from the chamber and the distance L between dots was measured. The actual in-situ axial stretch ratio was calculated as $\lambda_{in\ situ} = l_{in\ situ}/L$, whereby the reference length now corresponds to a state of no load and complete SMC relaxation. Accordingly, the axial stretch ratios λ_z applied in mechanical testing were calculated as $\lambda_z = l/L$. Five ring segments (1 mm width) were then cut from the central part of the fully relaxed arterial sample. A radial cut was applied to each ring, which was then placed in small volume of Krebs–Henseleit solution and given 30 min to mechanically equilibrate. The resultant geometry was close to a circular sector and was considered as the stress-free configuration of the arterial wall. The inner (L_i) and outer (L_o) arc lengths as well as thicknesses (H) of each sector were measured via analytical microscopy and used to calculate cross-sectional area (A) as follows:

$$A = \frac{H(L_o + L_i)}{2} \tag{1}$$

Making use of the incompressibility of the arterial tissue, the deformed inner radius (r_i) at each experimental state is calculated as

$$r_i = \sqrt{\frac{d_o^2}{4} - \frac{A}{\pi\lambda_z}} \tag{2}$$

By definition the pressure–diameter modulus E_p and compliance C are calculated as (Peterson et al., 1960)

$$E_p = \frac{\Delta P\, r_i}{\Delta r_i}\ C = \frac{\Delta r_i}{\Delta P\, r_i} \tag{3}$$

where Δr_i is the small increase in deformed inner radius caused by the small increase in pressure ΔP at the deformed configuration under given P and λ_z.

Theoretical framework

The arterial tissue is assumed to be an orthotropic incompressible elastic material, with axes of orthotropy in the radial (r), circumferential (θ), and axial (z) direction. The total Cauchy stress in the arterial wall is assumed as a sum of a passive stress with components σ_i^p, $i = r, \theta, z$ and an active stress that has components σ_θ^a and σ_z^a in the circumferential and axial direction. The passive stress is derived from the strain energy density function (SEF) which is a function of the principal Green strains $E_i = (1/2)(\lambda_i^2 - 1)$, $i = r, \theta, z$, where λ_i are the corresponding principal stretches. Because of the condition of material incompressibility, the components of the Green strain tensor are not independent but satisfy the condition $(2E_r + 1)(2E_\theta + 1)(2E_z + 1) = 1$. Using this equation E_r can be eliminated as an argument the SEF, i.e. $W = W(E_\theta, E_z)$. Following the approach for derivation of the passive constitutive relations given in (Rachev 2003; Humphrey, 2002), and in agreement with the introduced assumption for summation of the passive and active stress, the constitutive relations of the arterial tissue when the SMCs are stimulated to contract are

$$\sigma_\theta^c = \sigma_r + \lambda_\theta \frac{\partial W}{\partial \lambda_\theta} + \sigma_\theta^a, \qquad \sigma_z^c = \sigma_r + \lambda_z \frac{\partial W}{\partial \lambda_z} + \sigma_z^a, \tag{4}$$

where superscript c indicates the total stress under the contracted state. Because of material incompressibility the radial stress σ_r is unknown and has to be determined from the equations of equilibrium and boundary conditions.

Due to existence of residual strains in the unloaded ring tubular segment and the synergistic effects of the active stress, the stress and strain distributions across the arterial wall are close to uniform (Rachev and Hayashi, 1999). Therefore the mean values satisfactorily describe the stress and strain state. Hereafter the stresses and strains represent the mean values.

Consider two deformed states: one when the artery is relaxed (passive response), and another when the smooth muscle is stimulated to produce the so called isometric contraction. In the latter case the artery experiences the same circumferential stretch (and exhibits the same deformed inner and outer diameter) and the same axial stretch as in the passive response, but is inflated by different pressure. Though the contribution of the second term in the right hand side of Eq. (4) is the same in

Table 1 – Geometrical parameters of the zero stress configuration for each arterial sample, as well as the in-situ axial stretch ratio with preserved basal tone ($\lambda^{bt}_{in\text{-}situ}$) and in the fully relaxed smooth muscle cell state ($\lambda_{in\text{-}situ}$).

Sample	Outer arc-length(Lo) [mm]	Inner arc-length (Li) [mm]	Thickness (H) [mm]	$\lambda^{bt}_{in\text{-}situ}$	$\lambda_{z,\ in\text{-}situ}$
1	15.53	11.44	0.98	1.29	1.23
2	11.33	7.68	1.17	1.27	1.20
3	14.64	11.04	1.09	1.37	1.30
4	19.60	12.49	1.36	1.56	1.46
5	14.72	10.49	1.07	1.39	1.32
Average	15.17	10.63	1.13	1.38	1.30
SD	2.96	1.80	0.14	0.11	0.10

both deformed states, the stress states are different. The artery experiences different mean circumferential and axial stresses due to existence of active stresses (in the case of isometric contraction) and due to different mean radial stresses. The active axial stress can be calculated by subtracting the stress in the arterial wall when the SMCs are maximally relaxed from the total stress when the SMCs evoke isometric contraction, therefore

$$\sigma^a_\theta = \sigma^{ic}_\theta - \sigma^p_\theta + \sigma^p_r - \sigma^{ic}_r \quad \sigma^a_z = \sigma^{ic}_z - \sigma^p_\theta + \sigma^p_r - \sigma^{ic}_r \tag{5}$$

where the superscript *ic* signifies the isometric contracted state.

The mean values of wall stresses can be calculated directly from the experimental data as follows (Humphrey, 2002)

$$\sigma_r = -P\frac{r_i}{r_i + r_o} \qquad \sigma_\theta = P\frac{r_i}{r_o - r_i} \qquad \sigma_z = \frac{f}{\pi\,(r_o^2 - r_i^2)} \tag{6}$$

where r_o is the deformed outer radius. Then Eq. (5) yield

$$\sigma^a_\theta = \frac{2r_i r_o}{r_o^2 - r_i^2}(P_{ic} - P_p) \qquad \sigma^a_z = \frac{f_{ic} - f_p}{A} + \frac{r_i}{r_i + r_o}(P_{ic} - P_p) \tag{7}$$

where P_p and P_{ic} refer for the pressure in the case of passive response and isometric contraction, respectively.

The mean stretch ratios in the circumferential and axial direction are

$$\lambda_\theta = \frac{2\pi(r_o + r_i)}{L_o + L_i}, \qquad \lambda_z = \frac{l}{L} \tag{8}$$

where l is distance between markers in the current deformed state. Thus after processing the experimental pressure–diameter and extension-force data in the cases of the passive response and response under isometric contraction, it is possible to obtain active stress vs. principal stretch data. The analytical forms of the constitute relations $\sigma^a_\theta = \sigma^a_\theta(\lambda_\theta, \lambda_z)$ and $\sigma^a_z = \sigma^a_z(\lambda_\theta, \lambda_z)$ are proposed on the basis of certain experimental-based characteristics of the active response. Model parameters are quantified to yield the best-fit predictions of experimental stresses given by Eq. (7) by minimization of the objective functions

$$\Omega_\alpha = \sum_{n=1}^{N}\left(\frac{\sigma_\alpha^{a(teor)} - \sigma_\alpha^{a(exp)}}{\sigma_\alpha^{a(exp)}}\right)_n^2, \qquad \alpha = \theta, z \tag{9}$$

where $n = 1,2,\ldots N$ is the number of the experimental states.

The passive constitutive modeling follows a slightly modified methodology that has been used for quantification of strain energy function W from data of inflation-extension mechanical tests (Bellini et al., 2013). We adopt a four-fiber model for the passive mechanical properties, where the strain energy function is sought in the form (Bellini et al., 2013; Baek et al., 2007):

$$W = c(I_1 - 3) + \sum_{k=1,2,3,4}\frac{b_{1k}}{2b_{2k}}\left\{\exp\left[b_{2k}\left(\lambda_k^2 - 1\right)^2\right] - 1\right\}. \tag{10}$$

The first term accounts for the isotropic contribution of elastin (Zhou et al., 2014); c is a material constant, and $I_1 = \lambda_\theta^2 + \lambda_z^2 + (\lambda_\theta\lambda_z)^{-2}$ is the first invariant of the Cauchy–Green strain tensor. The second term includes the contribution of four families of collagen fibers. Subscript k denotes a family of collagen fibers oriented at a mean angle of α_k with respect to the longitudinal vessel axis; b_{1k}, and b_{2k} are material constants; and $\lambda_k = \sqrt{\lambda_\theta^2 \sin^2\alpha_k + \lambda_z^2 \cos^2\alpha_k}$ is the stretch ratio experienced by each family of collagen fibers due to deformation. The material constants c, b_{1k}, b_{2k} are determined by the minimization of an objective function based on constitutive representation given by Eq. (4) after setting $\sigma^a_\theta = \sigma^a_z = 0$,

$$\Omega_p = \sum_{n=1}^{N}\left(\frac{\hat\sigma^T_{\theta\,n} - \hat\sigma^E_{\theta\,n}}{\hat\sigma^E_{\theta\,n}}\right)^2 + \sum_{n=1}^{N}\left(\frac{\hat\sigma^T_{z\,n} - \hat\sigma^E_{z\,n}}{\hat\sigma^E_{z\,n}}\right)^2 \tag{11}$$

where

$$\hat\sigma^E_\theta = P_p\frac{r_i}{r_o - r_i} + P_p\frac{r_i}{r_o + r_i}, \qquad \hat\sigma^E_z = \frac{f_p}{\pi\,(r_o^2 - r_i^2)} + P_p\frac{r_i}{r_o + r_i}, \qquad \hat\sigma^T_\theta = \lambda_\theta\frac{\partial W}{\partial\,\lambda_\theta}, \qquad \hat\sigma^T_z = \lambda_z\frac{\partial W}{\partial\,\lambda_z}. \tag{12}$$

The superscripts E and T refer to the experimentally recorded and theoretically calculated values.

Results

Morphometric measurements of the porcine primary renal arteries in the stress-free configuration were obtained via image analysis (Table 1). Geometric variability among arteries might be due in part to the different age (7–12 month old) and weight of the pigs, although animal-specific information was not available for correlation. Experimental results show that complete SMC relaxation causes an increase in the traction-free sample length as compared to when the basal tone is preserved, i.e. $L^{bt}/L \approx 0.94$. The reported values of the in-situ axial stretch ratio account for this fact, with some variation noted among arterial samples (Table 1).

Representative pressure–outer diameter and axial force–pressure relationships at three values of the axial stretch for the cases of fully relaxed and maximally contracted SMCs are shown in Fig. 1. These plots illustrate the passive and total (passive and active) arterial response and the complex effects of deformations in the circumferential and axial directions. Error bars signify acceptable repeatability on measurements made on the same

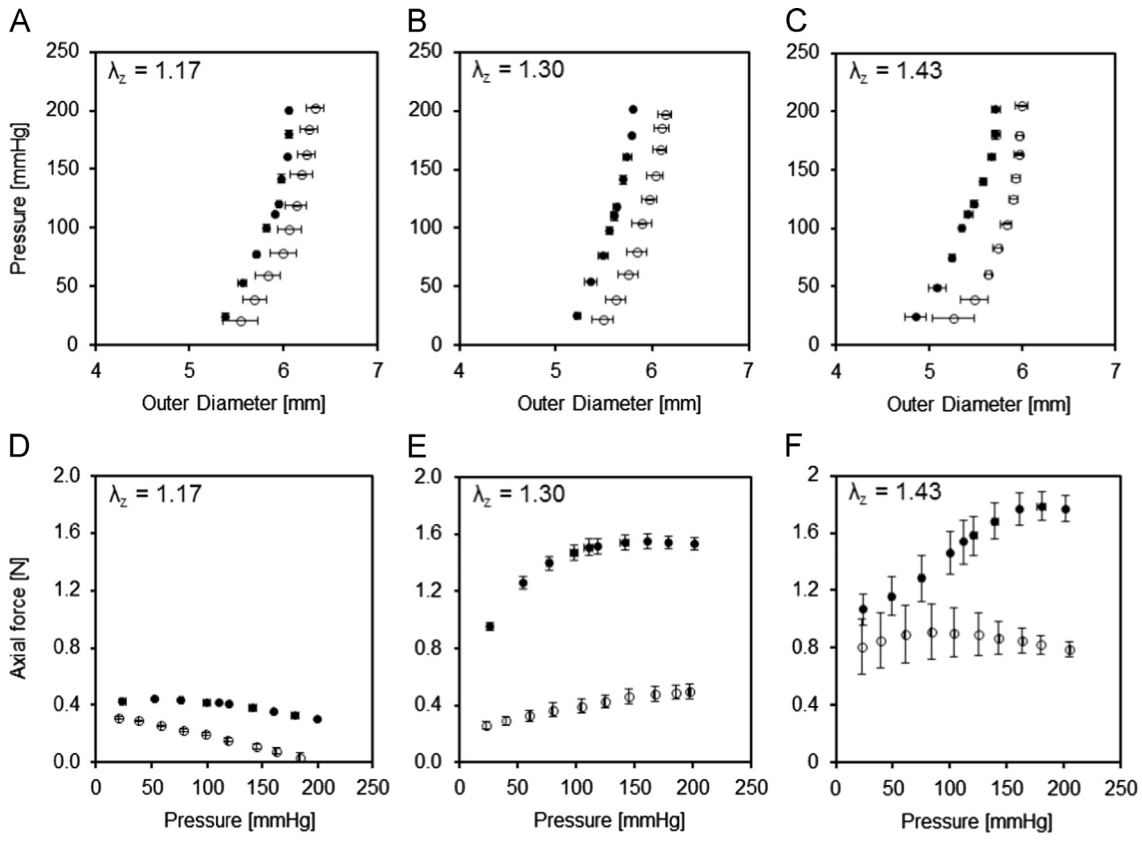

Fig. 1 – Pressure–deformed outer diameter (A–C) and axial force–pressure (D–F) relationships for a representative (sample 3, Table 1) porcine primary renal artery. The vessel mechanical response was recorded under conditions of maximally contracted (•) and fully relaxed (◦) smooth muscle cell states, and at three axial stretch ratios (λ_z) that span the in-situ value. Error bars represent the standard deviation of three repeat measurements on the same vessel.

vessel, and suggest that no damage was induced in the course of mechanical testing. Basic histological analyses were performed on a subset of vessels to verify that no notable damage was present in the vessel wall, and that the endothelium remained intact throughout mechanical testing. The passive pressure–outer diameter relationship is typical for muscular arteries, exhibiting non-linearity and monotonically increasing stiffness (J-shaped behavior) due to the relatively small elastin content in the vascular tissue (Fig. 1A–C) (Wagner and Humphrey, 2011). The pressure–diameter modulus calculated for in-situ axial stretch $\lambda_z = 1.3$ increases from $E_{P50} = 104.52 \pm 21.78$ *kPa* at pressure 50 mmHg to $E_{P100} = 223.69 \pm 5.89$ *kPa* at 100 mmHg and $E_{P200} = 353.14 \pm 14.57$ kPa at 200 mmHg. The moduli calculated at 100 mmHg and different stretch ratios are $E_{\lambda 1.17} = 108.84 \pm 2.95$ kPa, $E_{\lambda 1.30} = 223.69 \pm 5.89$ *kPa*, and $E_{\lambda 1.43} = 255.47 \pm 6.43$ kPa, which also show stiffening that is typically associated with increased axial stretch (Weizsacker and Kamp, 1990; Weizsacker and Pinto, 1988). The passive pressure–axial force relationships (Fig. 1D and E) shows that when axial stretch is at the in-situ value ($\lambda_z = 1.30$), the force is nearly constant over the pressure range 60–200 mmHg. The moderate force increase at in-situ axial stretch is similar to previous data reported for the porcine renal artery (Avril et al., 2013), and is in general agreement with experimental findings for rabbit basilar artery, which also belongs to the muscular vessel class (Wagner and Humphrey, 2011). The effects of axial stretch on the outer deformed diameter and axial force are shown in Fig. 2. As expected under constant pressure, an increase in the axial stretch causes a moderate shrinkage of the artery but significant augmentation of the axial force.

Muscle contraction modulates the mechanical response. When compared at equivalent pressures, the deformed diameter after stimulation of the SMCs (isobaric contraction) is smaller than the diameter in case of passive response (Fig. 1A–C). The active behavior remains J-shaped and the constricted artery exhibits higher stiffness than the relaxed artery compared at equivalent pressures. The corresponding pressure–diameter moduli at $\lambda_z = 1.3$ are $E_{P50} = 132.55 \pm 4.93$ kPa at 50 mmHg, $E_{P100} = 267.73 \pm 71.88$ kPa at 100 mmHg and $E_{P200} = 406.35 \pm 120.88$ kPa at 200 mmHg. Muscle contraction also induces a significant increase in the axial force (Fig. 1D–F).

The total circumferential and axial stresses developed with or without SMC activation are shown in Fig. 3. The passive circumferential or axial Cauchy stress significantly increases when the corresponding circumferential or axial stretch increases. However, the cross effects of λ_z on σ_θ and λ_θ on σ_z are less pronounced, similar to reported results for other types of arteries (Bersi et al., 2014). When the SMCs are stimulated to contract, the cross effects between stress and stretch are enhanced (Fig. 3).

Data for the passive stresses were used for identification of a constitutive formulation of the mechanical properties of the arterial tissue when the SMCs are maximally relaxed. The

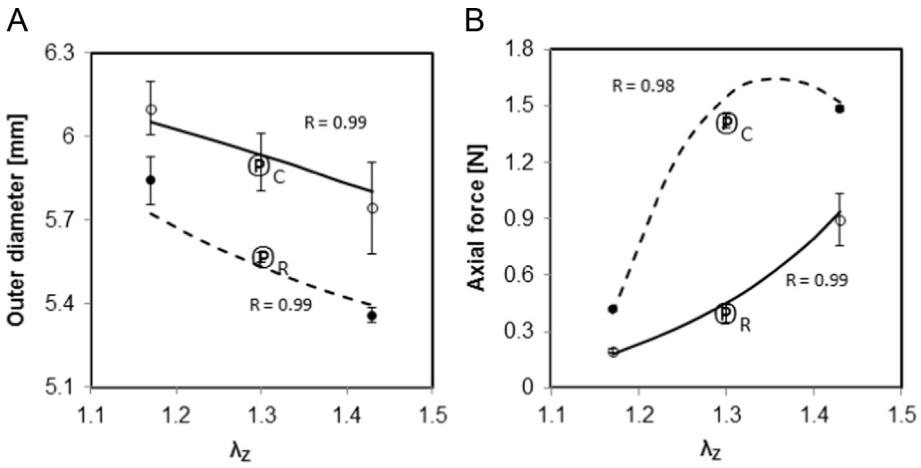

Fig. 2 – Representative (sample 3, Table 1) deformed outer diameter–axial stretch (A) and axial force–axial stretch (B) relationships under conditions of maximally contracted (•) and fully relaxed (◦) smooth muscle cell states. Data points indicate values interpolated from experimental data for $P=100$ mmHg, while solid/dashed lines indicate theoretical predictions. The P_C and P_R represent interpolated experimental points corresponding to $\lambda_z=\lambda_{in\text{-}situ}=1.3$ and $P=100$ mmHg while the smooth muscle cells are maximally contracted or fully relaxed, respectively. R values indicate correlation between experimentally recorded values and theoretical predictions. Error bars represent the standard deviation of three repeat measurements on the same vessel.

material constants of a four-fiber family strain energy function, Eq. (10), are obtained from the condition of the best fit between experimental and theoretical mean stresses, (Eq. (11)), and are given in Table 2. The model predictions for the passive stresses (continues curves in Fig. 3) are in good agreement with experimental data ($R \geq 0.93$ for the selected representative vessel).

The active stresses are decoupled from the passive stresses using Eq. (7), and the resultant data are displayed in Fig. 4. Stimulation of the vascular SMCs causes development of both circumferential and axial stress that depends on the stretches in a complex manner. The circumferential active stress increases almost linearly with increase in circumferential stretch, and the slope of σ_θ–λ_θ relation increases with axial stretch. The active axial stress manifests a non-monotonic relationship with axial stretch, and monotonically increases with circumferential stretch ratio over the range of experimentally recorded deformations (Fig. 4).

Motivated by the results shown in Fig. 4 and previously proposed constitutive formulations for the active stresses (Rachev and Hayashi, 1999; Agianniotis et al., 2012), we adopted the following analytical expressions:

$$\sigma_\theta^a = S_\theta(\alpha_\theta\lambda_z - 1)\lambda_\theta\left[1-\left(\frac{\lambda_{\theta\,\max}-\lambda_\theta}{\lambda_{\theta\,\max}-\lambda_{\theta\,o}}\right)^2\right]$$

$$\sigma_z^a = S_z(\alpha_z\lambda_\theta - 1)\lambda_z\left[1-\left(\frac{\lambda_{z\,\max}-\lambda_z}{\lambda_{z\,\max}-\lambda_{z\,o}}\right)^2\right] \quad (13)$$

S_θ and S_z are activation parameters that that depend on intensity of stimulation and spatial organization of the SMCs; $\lambda_{\theta\,\max}$ and $\lambda_{z\,\max}$ are the stretches where at fixed λ_z and λ_θ respectively, the active circumferential and axial stresses are maximal; $\lambda_{\theta\,o}$ and $\lambda_{z\,o}$ are the stretches below which no active stresses are developed; α_θ and α_z are material constants. A numerical surface fitting algorithm was used to calculate all model parameters and constants, with results given in Table 3. The theoretical vessel mechanical response (Fig. 2) and the active and total stress (Figs. 3–4) calculated form the identified analytical expressions agree well with experimental data ($R \geq 0.91$).

Discussion

This study focuses on the quantification of the active mechanical response of the porcine primary renal artery and constitutive formulation of the mechanical properties of the arterial tissue from in-vitro biaxial tests on tubular specimens. We recently quantified the strain energy function of the porcine primary renal artery using a 3-D approach (Zhou et al., 2014); in this study we again adopted a four-fiber family model but introduce a new 2-D approach. The 3-D approach accounts for a possible non-uniform distribution of the axial and circumferential stress across the arterial wall, which is most likely when an artery is considered as a thick-walled tube. In contrary, the classical 2-D approach considers the artery as a thin membrane which implies per se a uniform distribution of the tensile stresses and corresponding strains across the arterial wall (Wagner and Humphrey, 2011; Rachev, 2009). In this case the radial compressive stress is considered equal to zero across the wall despite the fact that this is true only at the outer arterial surface. As a result the passive stress is solely given by the second term in Eq. (4). The novel methodology for identification of the strain energy function proposed in the current study considers a uniform distribution of the circumferential and axial stresses but keeps the contribution of the mean radial stress (the first term in Eq. (4)). This is a special case of the 3-D approach, where validation does not require geometrical restrictions on the radius–thickness ratio, but rather a complete stress homogenization caused by the residual strains that exist in the traction-free configuration of an arterial segment.

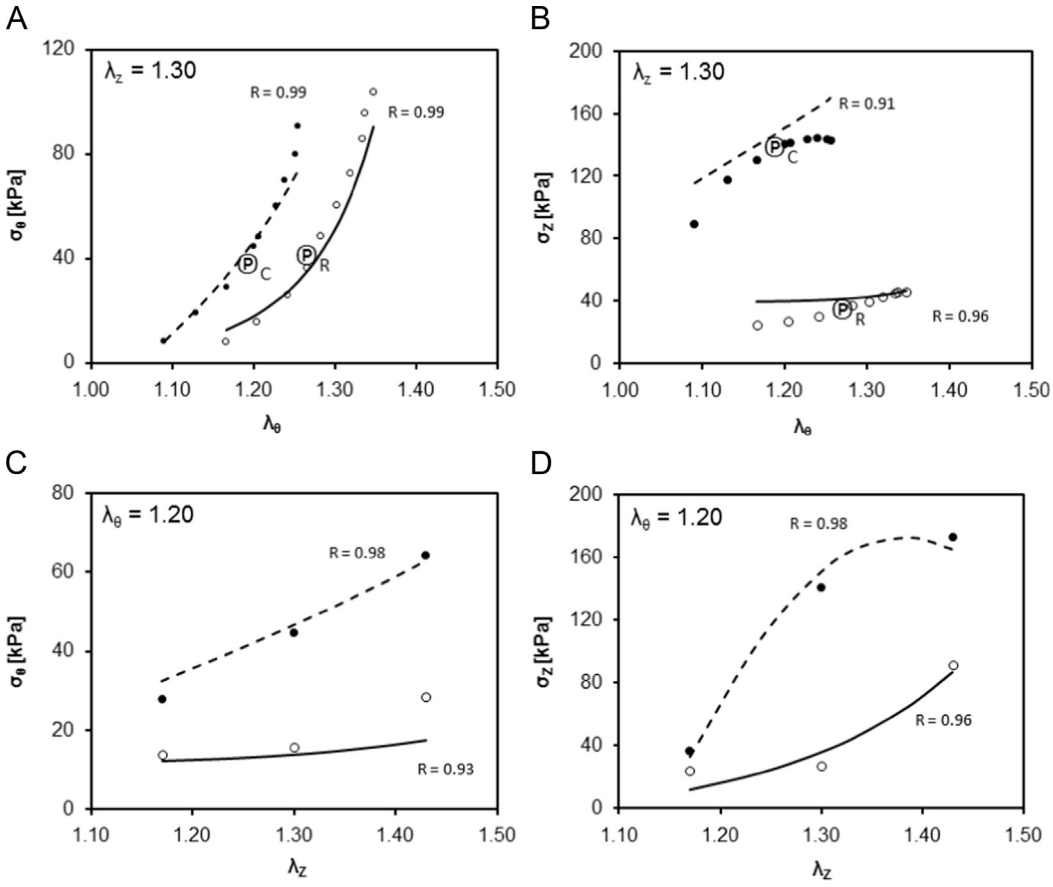

Fig. 3 – Representative (sample 3, Table 1) total stress–circumferential stretch (A and B) and total stress-axial stretch (C and D) relationships under conditions of maximally contracted (•) and fully relaxed (◦) smooth muscle cell states. Data points indicate experimentally recorded values, while solid/dashed lines indicate theoretical predictions. The Ⓟ$_C$ and Ⓟ$_R$ represent interpolated experimental points in the circumferential/axial stress–circumferential stretch planes corresponding to $\lambda_z=\lambda_{in\text{-}situ}=1.3$ and $P=100$ mmHg while the smooth muscle cells are maximally contracted or fully relaxed, respectively. R values indicate correlation between experimentally recorded values and theoretical predictions.

Table 2 – Best-fit parameters for the utilized structure-motivated strain energy function for the passive mechanical response.

Sample	b_0 [kPa]	b_{11} [kPa]	b_{12}	b_{21} [kPa]	b_{22}	b_{31} [kPa]	b_{32}	Alpha [°]	Residual
1	0.11	2.63	0.20	7.35	3.31	9.83	4.48	35.10	0.35
2	7.13	2.18	0.20	50.1	0.28	1.39	7.00	68.34	0.78
3	0.11	6.77	0.53	14.0	0.36	2.22	3.15	62.65	0.40
4	0.11	0.20	0.20	1.91	1.03	48.9	2.41	59.51	0.93
5	0.11	11.67	0.68	2.00	1.91	0.12	5.46	15.20	0.35
Average	1.51	4.69	0.36	15.1	1.38	12.5	4.50	48.16	0.56
SD	3.14	4.58	0.23	20.2	1.27	20.7	1.83	22.38	0.27

Experimental data for the passive arterial response are in agreement with available information for muscular arteries. In contrast to elastic vessels, such as the common carotid artery (Wagner and Humphrey, 2011; Gleason et al., 2004; Gleason and Humphrey, 2004), the structural stiffness of the renal artery monotonically increases with pressure. Under normal physiological load conditions (in-vivo axial stretch and pressure 100 mmHg) the mean circumferential and axial stresses are approximately 100–150 kPa (Fonck et al., 2007), while the mean radial stress is about 6.6 kPa. This means that accounting for the contribution of the radial stress when the circumferential or axial stresses are calculated from a strain energy function has a relatively minor impact (4.5–6.5%), however there is no reason to neglect this effect.

Constitutive formulation of arterial tissue mechanical properties requires that deformation measures such as stretches and strains are defined with respect to the stress-free sample configuration in absence of muscular tone. Thus in this study, the axial stretch is calculated with respect to the length of the traction-free tubular specimen when SMC contractility is abolished. Provided an artery manifests biaxial contractile properties, our approach negates the influence of

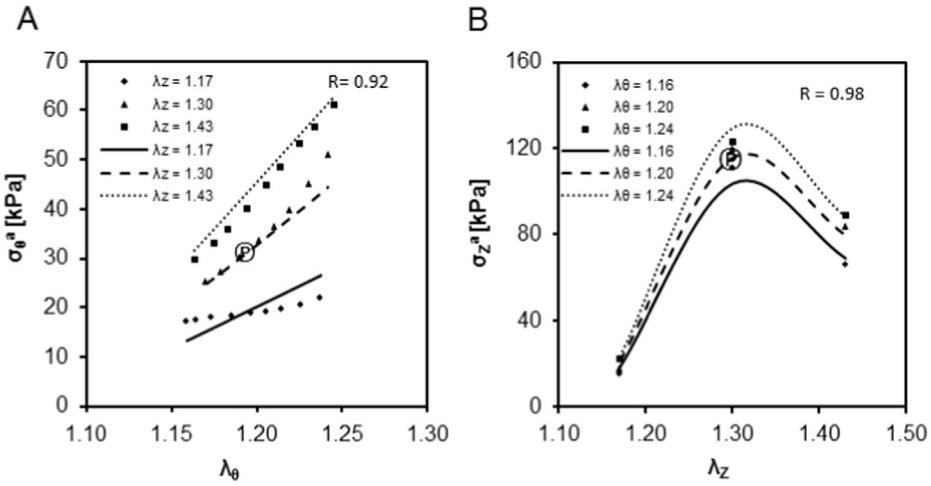

Fig. 4 – Representative (sample 3, Table 1) active circumferential stress–circumferential stretch relationships at three levels of axial stretch (A) and active axial stress–axial stretch (B) relationships at three levels of circumferential stretch. Data points indicate experimentally recorded values, while solid/dashed lines indicate theoretical predictions. The Ⓟ represents an interpolated experimental point in each stress–stretch plane corresponding to $\lambda_z=\lambda_{in\text{-}situ}=1.3$ and $P=100$ mmHg. R values indicate correlation between experimentally recorded values and theoretical predictions.

Table 3 – Best-fit parameters and resultant correlation with experimental data (R) for the proposed model of the active stresses.

Sample	S_θ [kPa]	α_θ	$\lambda_{\theta\ max}$	$\lambda_{\theta\ 0}$	R	S_z [kPa]	α_z	$\lambda_{z\ max}$	$\lambda_{z\ 0}$	R
1	295	0.95	1.56	0.68	0.99	98.0	2.10	1.27	1.10	0.98
2	295	0.99	1.42	0.97	0.79	175	1.14	1.26	1.08	0.99
3	308	1.04	1.98	1.08	0.92	235	1.15	1.32	1.15	0.99
4	295	0.83	1.61	0.67	0.86	42.8	2.10	1.46	1.33	0.93
5	298	0.83	1.25	1.08	0.76	80.1	1.40	1.34	1.28	0.98
Average	298	0.93	1.56	0.90	0.86	126	1.58	1.33	1.19	0.97
SD	5.72	0.09	0.27	0.21	0.09	77.8	0.49	0.08	0.11	0.02

basal tone on the traction-free tubular specimen length and therefore overestimation of the axial stretch.

It seems that the only published experimental results about the active properties of the renal artery are included in a paper by Cox, in which the author compares the passive and active response of six types of canine arteries (Cox, 1978). Despite a slightly different manner of experimental data presentation, our results confirm that under physiological loads the renal artery develops a circumferential active stress that is higher than the passive stress (Figs. 3 and 4). Our results show a monotonic, close to linear, increase in active circumferential stress with circumferential stretch up to pressures of 200 mmHg, while Cox reported a similar relationship for pressures only in the physiological range. The discrepancy might be caused by the inter species difference, the experimental protocols, and different method for calculation of the active stress.

The experimental data show that when compared at equivalent strains (isometric contraction, not shown) or equivalent pressures (isobaric contraction), the constricted artery exhibits higher pressure–diameter modulus compared to the dilated artery. Because of the assumed summation of the passive and active circumferential stress, an increase in the pressure–diameter modulus in the case of isometric contraction is fully expected. In the case of isobaric contraction however, predicting the effects of contraction on arterial structural stiffness is not straightforward. Peterson's modulus depends on the deformed geometry of the artery and on the incremental circumferential stress–strain modulus that describes the linearized mechanical behavior of the tissue at a specific deformed state. Increases in thickness/radius ratio and/or the incremental modulus lead to higher values for Peterson's modulus. SMC contraction constricts the artery and thus increases the thickness/radius ratio compared to the dilated vessel. Under equivalent loads, the constricted artery experiences smaller circumferential strain compared to the dilated vessel and therefore the "passive" part of the incremental modulus decreases. On the other hand due to contraction, the total incremental modulus has in addition an "active" part. Thus, the contraction-induced increase in Peterson's modulus in our study is the net result of geometrical and mechanical effects.

One of the mechanisms that regulate the muscular tone is the shear stress-dependent production of nitric oxide (NO) by the endothelial cells, which causes SMC relaxation. In the case of endothelial dysfunction, the reduced production of NO leads to an increase in muscular tone in concert with elevated blood pressure (Nava and Luescher, 1999). Results of

our study show that in the primary renal artery, elevated pressure and increased muscular tone synergistically enhance arterial stiffness, which in turn increases the risk of development and progression of cardiovascular diseases.

We found that stimulation of the SMCs generates not only circumferential but also axial stress. Because of the lack of information for the microstructure of the arterial wall, we proposed two independent phenomenological equations (Eq. (13)) for the active stresses that agree well with the experimental data. Decoupling the active and passive response facilities the selection of the analytical form of these equations because the dependence of active stresses on stretches is explicitly illustrated (Fig. 4). Following the described approach we selected a parabolic dependence of the circumferential (axial) active stress on the corresponding circumferential (axial) stretch. The linear dependence of the active stress on the other stretch (cross dependence) was found as a best fit among several functions.

The existence of biaxial active stress might have several plausible explanations that are not mutually exclusive. The dependence of active stresses on both the circumferential and axial stretches implies that SMCs might be oriented in the circumferential and axial direction, unless the cells themselves exhibit a biaxial active response. Another option is that all or at least some of the SMCs are helically-oriented within the arterial wall, a notion that is supported by previous histological observations of some arteries (Chen et al., 2013). Finally an explanation for the biaxial vasoactivity could be the rearrangement of collagen fibers when the SMCs are stimulated to contract. This means that in the case of isometric contraction the collagen is structurally organized in a different manner compared to the case of maximally relaxed muscle. Thorough histological investigations based on comparison between the arterial structures in the case of isometric contraction and maximally relaxed SMCs could shed light on this possibility.

The physiological significance of development an axial active stress is an open question. The following speculations about the mechanical stability of arteries provide a possible explanation. A free-body diagram of a portion of an artery (including the flowing blood) shows that it is subjected to two axial forces. One force is compressive and is equal to the product of arterial pressure and luminal area, $F_1 = P\pi r_i^2$, while the second force is tensile and is the resultant of the axial stress acting on the area of arterial cross-section $F_2 = \sigma_z \pi \left(r_o^2 - r_i^2\right)$. Under normotensive conditions the resultant of these forces is a tensile force and an artery considered as composite beam (cylindrical tube filled with incompressible fluid) is mechanically stable (Rachev, 2009). Focusing solely on the passive mechanical response, an increase in arterial pressure leads to increased luminal area and so both pressure and area collectively lead to an increase in the compressive force F_1. The tensile force F_2 remains virtually constant (Fig. 1E, open circles) and hence the probability that the artery could buckle is higher. It is well known that an elevation of arterial pressure is followed by an acute contractile response, termed the Bayliss effect. Due to arterial constriction the increase in compressive force F_1 is partially abolished, while due to developed active axial stress the tensile force F_2 increases (Fig. 1E, closed circles). Therefore the acute active response, including generation of the axial active stress, opposes the destabilizing effect of a short term increase in the arterial pressure.

Despite the novelty of some experimental findings and the encouraging predictive power of the proposed constitutive formulation of the biaxial active properties of the renal arteries, we recognize numerous limitations in our study. Our assessments were limited to the cases when the SMCs were completely relaxed or maximally contracted. There is a need of investigations on the renal artery active response under basal tone and at different levels of SMC stimulation. The potential for flow-induced shear stress to modulate SMC contraction via endothelial cell-mediated signaling was not considered. We did not account for the possible existence of longitudinal residual strains, which given the predominantly longitudinal orientation of elastin fibers observed in the renal artery (Kamenskiy et al., 2014) could be an appropriate refinement of the reference state from which strains are calculated. Moreover, this microstructure motivates the identification of models that account for the anisotropy of elastin as proposed in (Rezakhaniha et al., 2011). Finally, we did not account for the potential variance of in-situ renal artery dimensions due to respiration-induced movement of the kidney, which could impact the calculated in-situ pre-stretches (Hsiao et al., 2009).

Conclusion

Our obtained experimental results provide novel information on the biaxial active mechanical response of the primary porcine renal artery. The proposed constitutive model, developed in the framework of cardiovascular solid mechanics, provides theoretical active stress–stretch relations that agree well with experimental data. Our findings extend the current level of knowledge about arterial mechanics in a critical region of the circulatory system and demonstrate a robust experimental/theoretical methodology that can be applied to other muscular blood vessels. Future studies can advance beyond our data-motivated phenomenological approach through the development of bio-chemo-mechanical models for renal arteries.

Acknowledgements

This work was supported by the National Science Foundation/EPSCoR Grant (EPS-903795) and the National Institute of Health SC/INBRE Grant (P20 GM103499).

REFERENCES

Agianniotis, A., Rachev, A., Stergiopulos, N., 2012. Active axial stress in mouse aorta. J. Biomech. 45 (11), 1924–1927.

Avril, S., Badel, P., Gabr, M., Sutton, M.A., Lessner, S.M., 2013. Biomechanics of porcine renal arteries and role of axial stretch 2013. J. Biomech. Eng. 135 (8), 81007.

Baek, S., Gleason, R.L., Rajagopal, K.R., Humphrey, J.D., 2007. Theory of small on large: potential utility in computations of fluid–solid interactions in arteries. Comput. Methods Appl. Mech. Eng. 196, 3070–3078.

Bayliss, W.M., 1902. On the local reactions of the arterial wall to changes in internal pressure. J. Physiol. (London) 28, 220–231.
Bellini, C., Ferruzzi, J., Roccabianca, S., Di Martino, E.S., Humphrey, J.D., 2013. A microstructurally motivated model of arterial wall mechanics with mechanobiological implications. Ann. Biomed. Eng. 42 (3), 488–502.
Bersi, M.R., Ferruzzi, J., Eberth, J.F., Gleason, R.L., Humphrey, J.D., 2014. Consistent biomechanical phenotyping of common carotid arteries from seven genetic, pharmacological, and surgical mouse models. Ann. Biomed. Eng. http://dxdoi.org/10.1007/s10439-014-0988-6.
Brownlee, R.D., Langille, B.L., 1991. Arterial adaptation to altered blood flow. Can. J. Physiol. Pharm. 69, 978–983.
Cardamone, L., Valentin, A., Eberth, J.F., Humphrey, J.D., 2009. Origin of axial prestretch and residual stress in arteries. Biomech. Model. Mechanobiol. 8, 431–446.
Chen, H., Luo, T., Zhao, X., Lu, X., Huo, Y., Kassab, G.S., 2013. Microstructural constitutive model of active coronary media. Biomater. 34 (31), 7575–7583.
Cox, R.H., 1975. Arterial wall mechanics and composition and the effects of smooth muscle activation. Am. J. Physiol. 229, 807–812.
Cox, R.H., 1978. Regional variation of series elasticity in canine arterial smooth muscles. Am. J. Physiol. 234, H542–551.
Dartsch, P.C., Hämmerle, H., 1986. Orientation response of arterial smooth muscle cells to mechanical stimulation. Eur. J. Cell Biol. 41 (2), 339–346.
Dobrin, P.B., 1973. Influence of initial length on length–tension relationship of vascular smooth muscle. Am. J. Physiol. 225, 644–670.
Dobrin, P.B., 1978. Mechanical properties of arteries. Physiol. Rev. 58, 397–460.
Dobrin, P.B., 1983. Vascular mechanics. Chapter 3. In: Bohr, D.F., Somlyo, A.P., Sparks Jr., H.V. (Eds.), Handbook of Physiology. The Cardiovascular System. Vascular Smooth Muscle (Eds.) American Physiological Society, Bethesda, M.D., pp. 65–104.
Fonck, E., Prod'hom, G., Roy, S., Augsburger, L., Rüfenacht, D.A., Stergiopulos, N., 2007. Effect of elastin degradation on carotid wall mechanics as assessed by a constituent-based biomechanical model. Am. J. Physiol. Heart Circ. Physiol. 292 (6), H2754–H2763.
Gleason, R.L., Humphrey, J.D., 2004. A mixture model of arterial growth and remodeling in hypertension altered muscle tone and tissue turnover. J. Vasc. Res. 41 (4), 352–363.
Gleason, R.L., Taber, L.A., Humphrey, J.D., 2004. A 2-D model of flow-induced alterations in the geometry, structure, and properties of carotid arteries. J. Biomech. Eng. 126 (3), 371–381.
Holzapfel, G.A., Ogden, R.W., 2010. Constitutive modeling of arteries. Proc. R. Soc. A 466, 1551–1597.
Hsiao, H.M., Nikanorov, A., Prabhu, S., Razavi, M.K., 2009. Respiration-induced kidney motion on cobalt-chromium stent fatigue resistance. J. Biomed. Mater. Res. B: Appl. Biomater. 91 (2), 508–516.
Humphrey, J.D., 2002. Cardiovascular Solid Mechanics: Cells, Tissues, and Organs. Springer, New York.
Humphrey, J.D., Wilson, E., 2003. A potential role of smooth muscle tone in early hypertension: a theoretical study. J. Biomech. 36, 1595–15601.
Huo, Y., Cheng, Y., Zhao, X., Lu, X., Kassab, G.S., 2012. Biaxial vasoactivity of porcine coronary artery. Am. J. Physiol Heart Circ. Physiol, H2058–H2063.
Kamenskiy, A.V., Dzenis, Y.A., Kazmi, S.A., Pemberton, M.A., Pipinos, I.I., Phillips, N.Y., Herber, K., Woodford, T., Bowen, R. E., Lomneth, C.S., MacTaggart, J.N., 2014. Biaxial mechanical properties of the human thoracic and abdominal aorta, common carotid, subclavian, renal and common iliac arteries. Biomech. Model. Mechanobiol. 13 (6), 1341–1359.
Karšaj, I., Humphrey, J.D., 2012. A multilayered wall model of arterial growth and remodeling. Mech. Mater. 44, 110–119.
Kim, J., Wagenseil, J.E. (2014) Bio-Chemo-Mechanical Models of Vascular Mechanics, Annals of Biomedical Engineering, December.
Kockx, M.M., Wuyts, F.L., Buyssens, N., Van Den Bossche, R.M., De Meyer, G.R., Bult, H., Herman, A.G., 1993. Longitudinally oriented smooth muscle cells in rabbit arteries. Virchows Arch. A: Pathol. Anat. Histopathol. 422 (4), 293–299.
Matsumoto, T., Tsuchida, M., Sato, M., 1996. Change in intramural strain distribution in rat aorta due to smooth muscle contraction and relaxation. Am. J. Physiol. 271 (4 Pt 2), H1711–1716.
Nava, E., Luescher, T.F., 1999. Hypertension. In: Rubanyi, G.M. (Ed.), Pathophysiology and Clinical Applications of Nitric Oxide. Harwood Academic Publishers, Amsterdam, pp. 251–266.
Peterson, L.H., Jensen, R.E., Parnell, R., 1960. Mechanical properties of arteries in vivo. Circ. Res. 8, 622–639.
Rachev, A., 2003. Remodeling of arteries in response to changes in their mechanical environment. In: Holzapfel, G., Ogden, R. (Eds.), Biomechanics of Soft Tissue in Cardiovascular Systems. CISM Courses and Lectures, Course and Lecture No 441. Springer, Wien, New York, pp. 100–161.
Rachev, A., 2009. A theoretical study of mechanical stability of arteries. J. Biomech. Eng. 131, 051006-1–051006-9.
Rachev, A., Hayashi, K., 1999. Theoretical study of the effects of vascular smooth muscle contraction on strain and stress distributions in arteries. Ann. Biomed. Eng. 27 (4), 459–468.
Rezakhaniha, R., Fonck, E., Genoud, C., Stergiopulos, N., 2011. Role of elastin anisotropy in structural strain energy functions of arterial tissue. Biomech. Model. Mechanobiol. 10, 599–611.
Valentin, A., Humphrey, J.D., 2009. Modeling effects of axial extension on arterial growth and remodeling. Med. Biol. Eng. Comput. 47, 979–987.
Valentin, A., Cardamone, L., Baek, S., Humphrey, J.D., 2009. Complementary vasoactivity and matrix remodelling in arterial adaptations to altered flow and pressure. J. R. Soc. Interface 6, 293–306.
Vito, R.P., Dixon, S.A., 2003. Blood vessel constitutive models-1995–2002. Annu. Rev. Biomed. Eng. 5, 413–439.
Wagner, H.P., Humphrey, J.D., 2011. Differential passive and active biaxial mechanical behaviors of muscular and elastic arteries: basilar versus common carotid. J. Biomech. Eng. 133, 051009.
Weizsacker, H.W., Kamp, T.D., 1990. Passive elastic properties of of the rat aorta. Biomed. Tech. 35, 224–234.
Weizsacker, H.W., Pinto, J.G., 1988. Isotropy and anisotropy of the arterial wall. J. Biomech. 16 (703), 71.
Zhou, B., Wolf, L., Rachev, A., Shazly, T., 2014. A structure-motivated model of the passive mechanical response of the primary porcine renal artery. J. Mech. Med. Biol. 14 (3).